Uncertainty quantification of a spent fuel refrigeration pool utilizing a $k-\epsilon$ turbulence reduced order model

Jorge Yanez *, Andreas G. Class

Institute for Thermal Energy Technology and Safety, Karlsruhe Institute of Technology, Hermann-von-Helmholtz-Platz, 1, 76344, Karlsruhe, Germany

ARTICLE INFO

Keywords:
POD
Uncertainty quantification
ROM

ABSTRACT

In this article, the uncertainty of a three-dimensional turbulent natural convection transient is quantified in a geometry representing an idealized spent fuel pool. The assessment is carried out through the creation of a surrogate fast model. This is build utilizing Proper Orthogonal Decomposition and Galerkin projection applied to a K-ϵ turbulent Navier–Stokes formulation. We discuss the uncertainties created by a uncertain heat release of the spent fuel elements. We consider the hypothesis of deviations that follow the normal distribution around a certain nominal value, with different standard deviations and sample size. The expected results and its uncertainty are henceforth computed by Monte–Carlo method, calculating hundreds of solutions of the Initial Value Problem with the surrogate model.

1. Introduction

The prediction of nuclear reactor's thermal hydraulics relied in the past almost exclusively on experiments. In contrast, future developments and designs may count more intensively on numerical simulations.

With an enhanced usage of computational fluid dynamics (CFD), it is significant not only to obtain results, but also to assess its own statistical reliability. Additionally, for design and optimization it is relevant to analyze sensitivity of the layout on parameters, initial and boundary conditions.

In terms of Physics, the analysis of reactor's thermal hydraulics requires the study of convection. Several of the designs of fast reactors in actual development, i.e., the Lead-Cooled Fast Reactor, the Molten Salt Reactor and the Sodium-Cooled Fast Reactor (Alemberti et al., 2020; Merle-Lucotte et al., 2008; Moisseytsev and Sienicki, 2012), rely on natural convection of an non-compressible fluid for the residual heat removal in case of an emergency. The onset of the natural convection – from the operation forced regime – and the transients arising can be investigated utilizing a turbulent CFD calculation.

The extensive and exclusive usage of experiments for analysis of reactor's thermal hydraulics was not without grounds. Performing calculations, the accuracy of the results obtained – in conditions of potential instability – may be prone to bifurcation phenomena (Sheu and Lin, 2011). Under that circumstances, e.g. small divergences on the initial conditions may result in completely irrelevant aftermath. Therefore, a thorough assessment of the statistical trustworthiness of the numerical outcome is required to obtain conservative applicable results.

For the analysis of the convection, it is worth mentioning that the Standard k-ϵ model (Launder and Spalding, 1983) has been the workhorse for turbulent flow simulation since its creation in 1974. Its popularity has mean that it has been one of the most utilized methodologies for the simulation of turbulence in fluids. Conceptually, Standard k-ϵ model belongs to the Reynolds-Averaged Navier–Stokes (RANS) equations approach (Tennekes and Lumley, 1992), a common frames in which the equations of fluid are time-averaged. Several other models belong to this category. Among others, we may cite the k-ω model (Wilcox, 1988), the Re-Normalisation Group k-ϵ model (Yakhot et al., 1992) and the Shear Stress Transport turbulence model (Menter, 1994). In spite of the existence of these more modern models, Standard k-ϵ model, remains available in OpenFOAM (Weller et al., 1998) or Star-CCM (Siemens, 2018).

Independently of the kind of turbulence modeling we are considering and of the model we are utilizing, CFD calculations share a common characteristic: its deterministic nature. This feature implies that the statistical trustworthiness of the results cannot be assessed. For the matters incumbent to this study we may mention that CFD calculations disregard: (a) the accuracy of the simulation parameters, such as: dimensionless numbers, input or operational conditions, etc; (b) the bias and the unavoidable random variation of the realistic initial conditions compared with the nominal.

We may now illustrate the problematic enunciated before with an example. Consider an initial value problem in which real conditions are similar but not exactly the same as the nominal considered in the

* Corresponding author.

E-mail addresses: jorge.yanez@kit.edu (J. Yanez), andreas.class@kit.edu (A.G. Class).

analysis. Since only a single result is obtained, the confidence interval of the solution remains unknown. The effect of a small, but certain, initial divergence in the final solution remains an arcane. Actually, it cannot be mathematically stated that such small error in the initial conditions does not have a significant effect on the final result. The discrepancy may even trigger bifurcation (Drazin and Drazin, 1992) phenomena. That is, a minimal discrepancy, may make the solution to converge to another completely different result.

A strategy to address these matters simultaneously – error quantification, parameter sensitivity, initial condition sensitivity –, is to create a very fast model and run it in numerous varying cases. This surrogate model is called Reduced Order Model (ROM) (Quarteroni et al., 2014). Among other methodologies, those can be obtained utilizing the Proper Orthogonal Decomposition (POD) and Galerkin Projection. Very briefly summarized, the POD-Galerkin ROM methodology lie in computing a set of solutions with a CFD and post process them to find a reduced base. To finalize, simply project the governing equations in this new coordinate system. Since the methodology is mostly a clever change of basis, the procedure is mathematically sound, transformed equations are still derived from first principles, and the computation is quite fast and accurate.

The suitability of the methodology for uncertainty quantification and parametric studies has not remained unremarked and POD has been widely utilized (Hesthaven et al., 2016; Quarteroni et al., 2015). For a very recent, encyclopedic state of the art in the field we refer to the novel (Benner et al., 2021, 2020a,b). In the field of thermal-hydraulics with interesting applications for the nuclear industry we may cite, among others (Star et al., 2021a; Vergari et al., 2020; Star et al., 2021b; Yanez and Class, 2021b; Escanciano and Class, 2019; Yanez and Class, 2021b,a). POD is also suitable for investigation of applied fast reactors problems. In one hand the approach does not have restrictions in terms of spatial resolution. On the other hand, because of its promptitude, it provides the speed to analyze the possible bifurcations by massive force, through a Monte Carlo method (Sobol, 2018).

Therefore, and taking into account all previous considerations, we devote this document to the POD-Galerkin ROM for the standard k-ϵ model. The creation of a POD-Galerkin methodology for this turbulence model is a complicated task that we endeavored in Yanez and Class (2022). The complexity is due to the non-linearity of the equations, that poses a serious challenge for the development of a ROM. Those difficulties nevertheless were addressed mostly by the heuristic usage of the Discrete Empirical Interpolation Method (DEIM) (Chaturantabut and Sorensen, 2010), following the procedure described in Yanez and Class (2022).

With our methodology and construct ready, we apply our model for the investigation of the transient phenomena of natural convection (Grishchenko et al., 2015). We employ our construct with an idealized spent fuel pool, a similar – but more simplified – facility as the ones investigated in Wang et al. (2012), Hung et al. (2013), Jang et al. (2006) and Galik et al. (2016). This is relevant for the design of refrigeration pools for nuclear industry (Abderrahim et al., 2010).

We carry out our study to asses the accuracy of the results that can be obtained in case some impreciseness is present in the heat released by burned fuel elements. This inaccuracy may be due to an inadequate determination of the usage of the element, human error of the operator selecting the element, etc.

In spite of the fact that we apply our model to a very idealized spent fuel pool, since the construct created applies to any convective system with heat and momentum sources/sinks, we want the set the emphasis of the study in the feasibility of the method. We illustrate the performance of the model, demonstrating the viability of a uncertainty quantification study by a POD model of a RANS calculation. We derive mean, standard deviation as well as the accuracy of the last by performing calculations, feasible in short times with different sample sizes, studying the computational performance of the model.

2. ROM

The ROM is derived originally from the incompressible and dimensionless Navier–Stokes equations utilizing the Boussinesq approximation. Such system is complemented with the k-ϵ equations. Utilizing the Einstein notation,

$$\frac{\partial u_i}{\partial x_i} = 0, \tag{1}$$

$$S_t \frac{\partial u_i}{\partial t} + \frac{\partial u_j u_i}{\partial x_j} = \frac{1}{Re}\frac{\partial^2 u_i}{\partial x_j^2} - \frac{1}{\rho}\frac{\partial p}{\partial x_i} + \frac{Ra}{Re^2 Pr} T e_i - K\frac{1}{2}\left|\vec{u}\right| u_i - \frac{2}{3}\frac{\partial k}{\partial x_i} + \frac{\partial \nu_t}{\partial x_j}\frac{\partial u_i}{\partial x_j} + \nu_t \frac{\partial^2 u_i}{\partial x_j^2}, \tag{2}$$

$$S_t \frac{\partial T}{\partial t} + \frac{\partial u_j T}{\partial x_j} = \frac{1}{Re Pr}\frac{\partial}{\partial x_j}\left(\frac{\partial T}{\partial x_j}\right) + \frac{\dot{Q}}{c_p \rho}\frac{t_0}{T_1 - T_0} + \frac{S_t^2 v_0^2}{(T_1 - T_0)c_p} u_i \frac{1}{2} K \left|\vec{u}\right| u_i + \frac{1}{Pr}\frac{\partial \nu_t}{\partial x_j}\frac{\partial T}{\partial x_j} + \frac{1}{Pr}\nu_t \frac{\partial^2 T}{\partial x_j^2}, \tag{3}$$

$$\frac{\partial k}{\partial t} + \frac{\partial k u_i}{\partial x_i} = \frac{1}{Re}\frac{\partial^2 k}{\partial x_j^2} + \frac{1}{\sigma_k}\frac{\partial \nu_t}{\partial x_j}\frac{\partial k}{\partial x_j} + \frac{1}{\sigma_k}\nu_t \frac{\partial^2 k}{\partial x_j^2} + \nu_t S^2 + (T_1 - T_0)\frac{1}{Pr_t}\beta g_{dl} e_i \nu_t \frac{\partial T}{\partial x_i} - \epsilon, \tag{4}$$

$$\frac{\partial \epsilon}{\partial t} + \frac{\partial \epsilon u_i}{\partial x_i} = \frac{1}{Re}\frac{\partial^2 \epsilon}{\partial x_j^2} + \frac{1}{\sigma_\epsilon}\frac{\partial \nu_t}{\partial x_j}\frac{\partial \epsilon}{\partial x_j} + \frac{1}{\sigma_\epsilon}\nu_t \frac{\partial^2 \epsilon}{\partial x_j^2} + c_{1\epsilon}\frac{\epsilon}{k}\nu_t S^2 + (T_1 - T_0)c'_{3\epsilon}\frac{1}{Pr_t}\beta g_{dl} e_i \frac{\epsilon}{k}\nu_t \frac{\partial T}{\partial x_i} - c_{2\epsilon}\frac{\epsilon^2}{k}, \tag{5}$$

$$S_{ij} = \frac{1}{2}\left(\frac{\partial u_j}{\partial x_i} + \frac{\partial u_j}{\partial x_i}\right), \tag{6}$$

$$S^2 = 2 S_{ij} S_{ij}, \tag{7}$$

where u_i is the velocity, T the temperature, p pressure, ρ density, k the turbulent kinetic energy, ϵ the rate of dissipation of turbulent kinetic energy. The main scales of the problem are the main length L_0, time $t_0 = L_0^2/\kappa$ where κ is thermal diffusivity, velocity $v_0 = L_0/t_0$ and the two temperatures T_0 and T_1. x defines the length coordinate whilst i, j are the sub-indexes addressing the different directions. Additionally, K designate the resistant coefficient, ν_t the dimensionless turbulent viscosity (Inverse of Re_t), $\dot{Q}$ are the volumetric heat sources, c_p is the heat capacity at specific pressure, β the coefficient of thermal expansion, μ is the dynamic viscosity, g the module of the dimensionless acceleration of gravity and e its direction. $S_t = L_0/(v_0 t_0)$, Pr, $Re = \rho v_0 L_0/\mu$, $Ra = \rho^2 g \beta (T_1 - T_0) L_0^3/(\mu^2 Pr)$ are the Strouhal, Prandtl, Reynolds and Rayleigh numbers. The specific constants of the Standard k-ϵ model are $\sigma_k = 1$, $\sigma_\epsilon = 1.3$, $c_{1\epsilon} = 1.44$, $c_{2\epsilon} = 1.92$ and $c'_{3\epsilon} = 1$.

The extensive procedure carried out to obtain ROM of k-ϵ equations has been detailed on the publication (Yanez and Class, 2022). Therefore, we just sketch the procedure for completion and describe the points were minor differences exist with that reference.

The derivation procedure consist of three stages: (a) computation of the reduced basis; (b) projection of the equations in the new basis; (c) the so called *hyper-reduction*, i.e. the process intended to deal efficiently with non-linear terms.

2.1. Reduced basis computation

We utilize the *Method of Snapshots* (Berkooz et al., 1993) to obtain a reduced basis. we apply it separately to each variable, v, T, k, ϵ. That is, we obtain solutions y of k-ϵ equations with the high fidelity solver STAR-CCM at times $\{t_1, \ldots, t_n\}$ for a set of initial value problems $\{y_1(0,x), \ldots, y_m(0,x)\}$. Note that we shall define the geometry and boundary conditions of the case as well as the selected initial value conditions later, in the following sections of this document. Also, we consider the one parametric H^1 Sobolev inner product, $\langle f, g\rangle_{\delta_s} = \int_\Omega f g d\Omega + \delta_s \int_\Omega \partial_i f \partial_i g d\Omega$, where δ_s is a small positive parameter and f and g generic function.

Therefore, we form matrix Y,

$$\begin{bmatrix} y_1(t_1,x) & y_1(t_2,x) & \dots & y_1(t_n,x) \\ \sqrt{\delta_s}\partial_x y_1(t_1,x) & \sqrt{\delta_s}\partial_x y_1(t_2,x) & \dots & \sqrt{\delta_s}\partial_x y_1(t_1,x) \\ \sqrt{\delta_s}\partial_y y_1(t_1,x) & \sqrt{\delta_s}\partial_y y_1(t_2,x) & \dots & \sqrt{\delta_s}\partial_y y_1(t_1,x) \\ \sqrt{\delta_s}\partial_z y_1(t_1,x) & \sqrt{\delta_s}\partial_z y_1(t_2,x) & \dots & \sqrt{\delta_s}\partial_z y_1(t_1,x) \end{bmatrix} \dots$$
$$\dots \begin{bmatrix} y_j(t_1,x) & y_j(t_2,x) & \dots & y_j(t_n,x) \\ \sqrt{\delta_s}\partial_x y_j(t_1,x) & \sqrt{\delta_s}\partial_x y_j(t_2,x) & \dots & \sqrt{\delta_s}\partial_x y_j(t_1,x) \\ \sqrt{\delta_s}\partial_y y_j(t_1,x) & \sqrt{\delta_s}\partial_y y_j(t_2,x) & \dots & \sqrt{\delta_s}\partial_y y_j(t_1,x) \\ \sqrt{\delta_s}\partial_z y_j(t_1,x) & \sqrt{\delta_s}\partial_z y_j(t_2,x) & \dots & \sqrt{\delta_s}\partial_z y_j(t_1,x) \end{bmatrix} \dots$$
$$\dots \begin{bmatrix} y_m(t_1,x) & y_m(t_2,x) & \dots & y_m(t_n,x) \\ \sqrt{\delta_s}\partial_x y_m(t_1,x) & \sqrt{\delta_s}\partial_x y_m(t_2,x) & \dots & \sqrt{\delta_s}\partial_x y_m(t_1,x) \\ \sqrt{\delta_s}\partial_y y_m(t_1,x) & \sqrt{\delta_s}\partial_y y_m(t_2,x) & \dots & \sqrt{\delta_s}\partial_y y_m(t_1,x) \\ \sqrt{\delta_s}\partial_z y_m(t_1,x) & \sqrt{\delta_s}\partial_z y_m(t_2,x) & \dots & \sqrt{\delta_s}\partial_z y_m(t_1,x) \end{bmatrix}. \tag{8}$$

We carry out the Singular Value Decomposition, $Y = V\Sigma G^T$. V is an orthogonal matrix that allow to project the n dimensional vector space in a reduced–subspace of dimension $n - j$ dropping the last j vectors in V. Note that mall parameter of Sobolev inner product (Iollo et al., 2000) was determined in the same manner as it has been performed in Escanciano and Class (2019) and Yanez and Class (2021b,a).

As this stage it is pertinent to mention that we have post-process the solutions, to compute the gradients, externally with a self-developed code. We are carrying a completely non-intrusive approach, since the commercial code utilized is completely closed for the authors.

2.2. Projection of the equations

We rewrite our system of equations into a variational formulation, in terms of the reduced order basis. We follow a Galerkin formulation, thus, we express test and trial functions in terms of the same reduced order basis. Note also, that we utilize H^1 inner product to derive variational formulation. To do this, we follow the now conventional procedure described in e.g. Quarteroni et al. (2015), in the same manner as in our previous publications (Escanciano and Class, 2019; Yanez and Class, 2021b,a,b).

2.3. Hyperreduction

At this stage with the determination of the non-linear variables, the ROM is closed. For Standard k-ϵ model those are $|u|$, k^2/ϵ and ϵ/k. The Discrete empirical interpolation method (DEIM) (Quarteroni et al., 2015; Chaturantabut and Sorensen, 2010) allows treating such variables efficiently.

DEIM consists of calculating the values of the non-linear magnitudes in the CFD results. Then, apply the Method of Snapshots to this database to derive a reduced basis of the non-linear variable. The amplitudes of the non-linear variables in its own reduced basis can be then obtained. To do so, the values of the non-linear variable is calculated in a reduced set of points which cardinality is equal or larger (but of similar order) than the reduced basis of the non-linear magnitude. The amplitudes can be obtained resolving a linear system, over-determined or not, depending on the amount of points.

Pitifully, the application of DEIM – now a conventional method, ology – to the problem in hand is not straightforward. This has to do with the rational nature of the functions k^2/ϵ and ϵ/k. Note that both k and ϵ take very small values in some domains. Tiny inaccuracies in the denominator can result in a value for the non-linear variable that invalidate the DEIM procedure. Those inaccuracies are not fortuitous. The small mistakes originated by the ROM combined with the numerical discrepancies coming from the CDF and the deficiencies of the standard k-ϵ model generate them steadily in certain regions. The heuristic procedure to overcome this severe deficiency has been the main object of our paper (Yanez and Class, 2022), and refer the readers to this reference for further details.

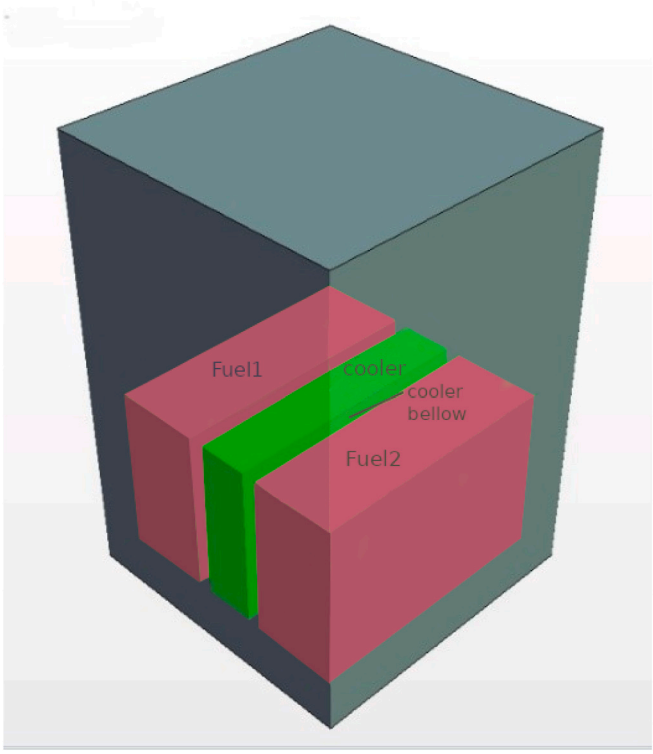

Fig. 1. Sketch of the geometry.

2.4. Final model

This process culminates in the final numerical system,

$$\left(\mathbb{D} + \frac{\Delta t}{2}\mathbb{E}\right)\begin{pmatrix}\vec{\delta u}\\ \vec{\delta T}\\ \vec{\delta k}\\ \vec{\delta \epsilon}\end{pmatrix} - \Delta t\mathbb{G} = 0. \tag{9}$$

Note that $\mathbb{D}$, $\mathbb{E}$, $\mathbb{G}$ are matrices – for their exact form see Yanez and Class (2022) – dependent on the dimensions of the reduced basis only. Also, note that they should partially recalculated every time step of the integration procedure.

3. Problem

We apply our ROM to investigate the transients of natural convection (Grishchenko et al., 2015) into a simplified spent fuel refrigeration pool. The facility is represented by the gray cuboid of 4 × 4 × 5.8 m shown in Fig. 1. It is considered to be isolated, so that all variables have a gradient equal to zero in the direction perpendicular to the walls.

The volume is filled with water, which is considered to have constant properties, with density 997 $\mathrm{kg\,m^{-3}}$, specific heat 4200 $\mathrm{J\,kg^{-1}\,K^{-1}}$ and heat conductivity 0.0269 W/m/K.

The decay heat of the spent fuel elements is considered as two volumetric heat sources of 1 $\mathrm{MW\,m^{-3}}$ shown in magenta in the figure. In the center, marked in green, two smaller parallelepipeds that represent volumetric sinks are located vertically aligned one above the other. The upper one is disconnected, whilst the lower sink removes −2.3 $\mathrm{MW\,m^{-3}}$. Heat sources and losses occur directly in water.

We consider the problem initially at rest, a moment in which the sources and sinks are set up and the simulation started. As a high fidelity solver, we utilize STAR-CCM version 2020.3. After 150 s, some flow has been established, but the problem is still far from stationary conditions. The situation at this stage can be seen in Figs. 2(a)–3(b).

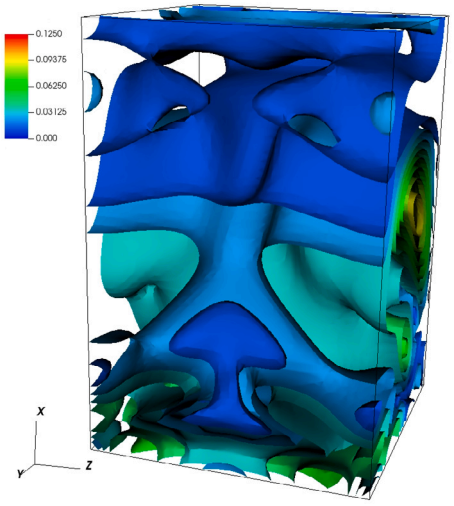

(a) Velocity, $\mathrm{m\,s^{-1}}$.

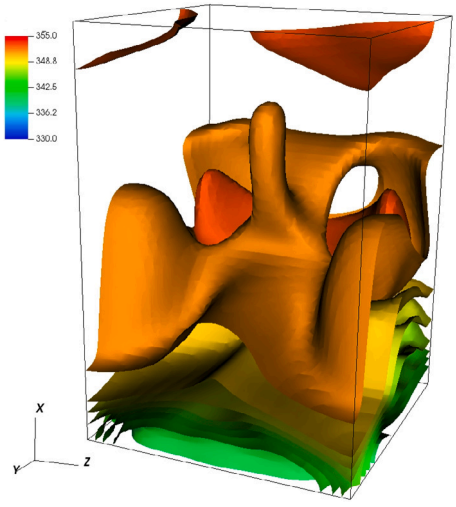

(b) Temperature, values in K.

Fig. 2. Fields at 150 s.

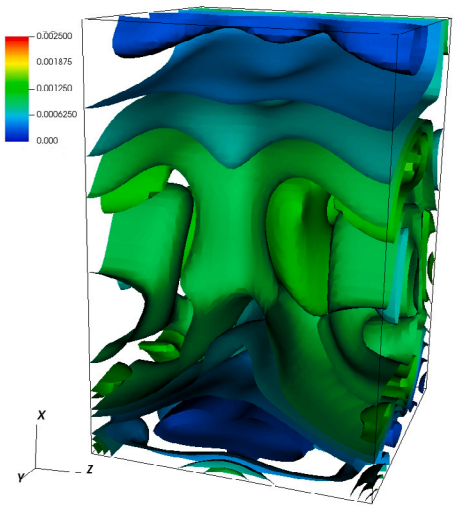

(a) k, values in $\mathrm{m^2\,s^{-2}}$.

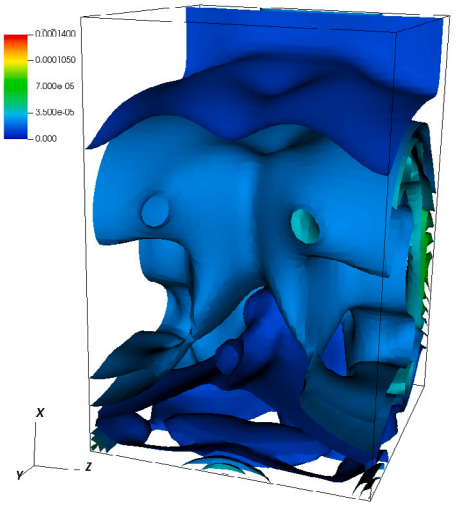

(b) ϵ, values in $\mathrm{m^2\,s^{-3}}$.

Fig. 3. Fields at 150 s bis.

The flow still has transients which are the main interest of the simulation. After this moment, we make several runs –at conditions that will be detailed later, in Section 4.1– with the CFD collecting snapshots every second for the next 50 s, between 150 s and 200 s. In each run, we regard the decay heat of the spent fuel elements as the parameter of our study. Therefore, we vary this magnitude, considering ratios of the thermal output.

4. Uncertainty quantification

4.1. Description of the parametric experiment

We consider the heat sources intensities $\dot{Q}$ in Eq. (3) as the parameter of our statistical experiment. We consider the following hypothesis for our statistical experiment. We define the values of $\dot{Q}$ combining the nominal conditions corresponding to the high fidelity calculation appearing in Yanez and Class (2022), $\dot{Q}_0$ with a perturbation. We consider perturbations following a Truncated Normal distribution (Kroese et al., 2013) centered in the design values. We clip the distribution in values corresponding to 0% and 200% of the nominal amplitudes. We also regard each of the perturbations to be completely uncorrelated with the others. Summarizing, the occurrence i of the decay heat of the spent fuel is

$$\dot{Q}_i = N_{tr}(\mu, \sigma, a, b) \cdot \dot{Q}_0. \tag{10}$$

Here we have considered N_{tr} is the truncated normal distribution, $\mu = 1$ is the design average of 100% of the nominal output, σ is the standard deviation, and the parameters $a = (\mathrm{clip}_{low} - \mu)/\sigma$, $b = (\mathrm{clip}_{high} - \mu)/\sigma$, are so related to the intended clipping of $\mathrm{clip}_{low} = 0\%$ and $\mathrm{clip}_{high} = 200\%$.

4.2. CDF calculations

At this stage, it is necessary to define which CFD calculations should be carried out in order to cover the range $[0\%, 200\%]$ of the nominal heat output in the domain 150 s to 200 s. The snapshots collected from these calculations will enrich the database from which the reduced basis will be derived. Per definition, we have decided to consider the nominal value and the limits of the interval. Then we have added calculations to keep the *a posteriori* relative error of the ROM – defined later in Section 4.3 – under the value of 5%. Note that this magnitude encloses the divergences due to the reduced basis plus the inherent

deviations of the ROM integration. It is derived utilizing a double threshold of mistake for the derivation of the reduced database (Yanez and Class, 2021b). A small trial and error procedure has allowed us to conclude that CFD calculations every 25% allow us to achieve the desired accuracy. In an *abstract* manner, we have formed a matrix constituted by calculation vectors in the following way

$$\begin{aligned}&\left(\mathrm{CFD}_{0\%}, \mathrm{CFD}_{25\%}, \mathrm{CFD}_{50\%}, \mathrm{CFD}_{75\%}, \mathrm{CFD}_{100\%},\right.\\&\left.\mathrm{CFD}_{125\%}, \mathrm{CFD}_{150\%}, \mathrm{CFD}_{175\%}, \mathrm{CFD}_{200\%}\right).\end{aligned} \tag{11}$$

The j index of formula (8) corresponds to each of the entries of vector (11). A total of 450 snapshots have been collected.

In this study, the relevance of the results of the CFD in terms of verification and validation is a working hypothesis. We concentrate on the creation and usage of the ROM so that statistical magnitudes can be extracted from the analysis.

4.3. Reduced basis

The reduced basis is obtained utilizing the procedure discussed in Section 2.1. The post-processing of the snapshots considering a maximum distance of 10^{-6} to the projection space provides dimensions $(J_u, J_T, J_k, J_\epsilon) = (15, 9, 17, 20)$. Utilization of a second threshold, 10^{-7}, for the determination of the *a posteriori* error (Yanez and Class, 2021b,a) provides a projection space of an enhanced dimension $(J'_u, J'_T, J'_k, J'_\epsilon) = (24, 16, 26, 28)$.

We may make an estimate the *a posteriori* error E, and thus on the accuracy of the ROM, by

$$E_J^{J'} = \sqrt{\sum_{j=J}^{J'} u_j^2} \Big/ \sqrt{\sum_{j=1}^{J'} u_j^2}, \tag{12}$$

where the u_j are the amplitudes of an arbitrary variable. This is the magnitude we utilize to check the goodness of the set of CFD calculations in Section 4.2.

On the other hand, we may make a very simple assessment of the effectiveness of the reduced basis considering the *a priori* error of

$$\|(I - VV^T)f\|/\|f\|, \tag{13}$$

which provides the capabilities of the reduced database to reproduce the original values. Such assessment has been carried out for the variables u, T, k and ϵ in the Figs. 4(a)–5(b)

In those plots we have represented the values of the formula (13) for factors of the nominal output. Note that all the mistakes remain under 1.5%. Also see that in spite of the low values, the mistakes noticeable increase with time. Thus, for an enhanced result an augmentation of the CDF physical calculation time, maybe advisable. For the study in hand the level of mistake is wholly acceptable, and therefore, no expansion in time of the database has been considered.

4.4. Statistical magnitudes as a function of the reduced order model

4.4.1. Obtaining of the statistical parameters

To study the uncertainty quantification, we aim to obtain by an statistical procedure $\mathbb{E}(y(t,x))$ and $\sigma(y(t,x))$. For conciseness, in this section we consider that y is a generic variable with integration results u, with probability density $\rho(u)$, which has modes ϕ_i obtained for a set of parameters q_r. The amount of modes is J', the quantity of parameters N and the dimension of the CFD calculations is n. We utilize the Monte-Carlo method (Sobol, 1974, 2018) to derive these magnitudes. Since the output of the ROM are the amplitudes in the reduced basis we need to express the statistical magnitudes as a function of that quantities. Following Yanez and Class (2021b), the average can be expressed as,

$$\overline{y}(x,t) = \sum_i^{J'} \left(\frac{1}{N} \sum_r^N u_i(t, q_r) \right) \phi_i(x), \tag{14}$$

whist the variance expansion in terms of the modes is,

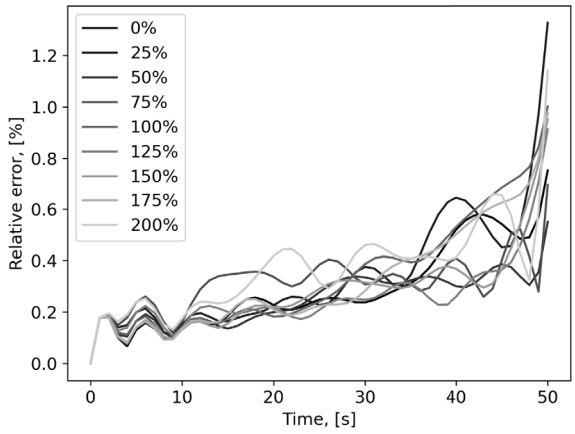

(a) Velocity

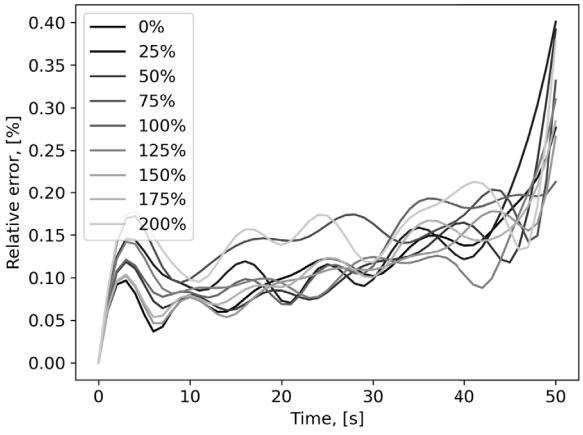

(b) temperature

Fig. 4. Achievable relative error of the database.

$$\sigma_y^2(x,t) = \frac{1}{N} \sum_r^N \left(\sum_i^{J'} \phi_i(x) \left(u_i(t,q_r) - \frac{1}{N} \sum_s u_i(t,q_s) \right) \right)^2. \tag{15}$$

The accuracy of the previous magnitudes is defined in terms of expectations. For the mean,

$$E_{av}(t,x) = \left| \int_Q \rho(q) u(t,x,q) dq - \frac{1}{N} \sum_r u(x,t,q_r) \right|. \tag{16}$$

To simplify the notation for further analysis we define $I(t,x) = \int_Q \rho(q) u(t,x,q) dq$ and $U(t,x) = {}^1/_N \left(\sum_r u(x,t,q_r) \right)$. The accuracy of the variance is,

$$\begin{aligned}E_{var}(t,x) = \Bigg| &\int_Q \rho(q) \left(u(t,x,q) - \mathbb{E}\left(y(t,x)\right) \right)^2 dq \\ &- \frac{1}{N} \sum_r \left(u(x,t,q_r) - \overline{y} \right)^2 \Bigg|,\end{aligned} \tag{17}$$

where we define $J(t,x) = \int \rho(u(x,t,x_0) - E(u)(x,t))^2 dx_0$, and $s^2(t,x) = {}^1/_N \left(\sum_k (u(x,t,x_{0k}) - E(u)(x,t))^2 \right)$. In Yanez and Class (2021b,a) we have already studied these expectations. The accuracy of the mean can be assessed by,

$$P\left(|I(t,x) - U(t,x)| < 3 \sqrt{\frac{\sigma^2_{\text{sample}}(u(x,t))}{N}} \right) \geq 0.997. \tag{18}$$

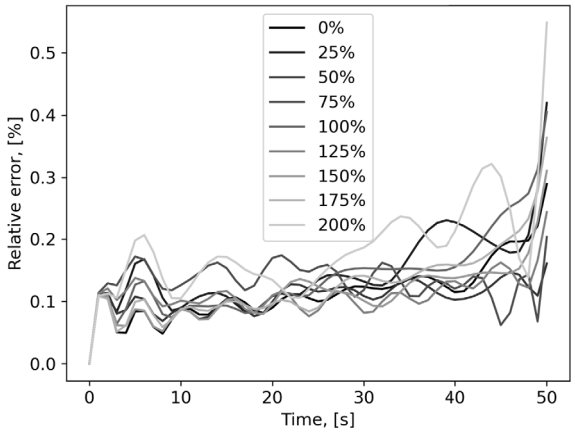

(a) k

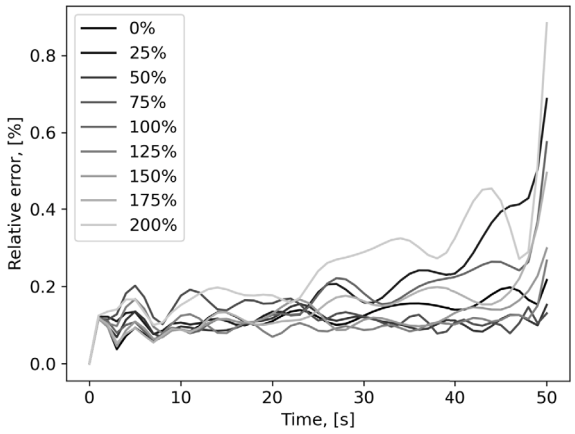

(b) ϵ

Fig. 5. Achievable relative error of the database, II.

For the standard deviation we have,

$$P\left(|\sqrt{J}(t,x)-\sqrt{s^2}(t,x)|\leq\sqrt{3}\sqrt[4]{\sigma^2_{sample}(s^2)/N}\right)>0.997. \tag{19}$$

The only remaining variable to be calculated is $\sigma^2(s^2)$. Two expressions for it were derived in Yanez and Class (2021b). In this study we recall the expression,

$$\sigma^2(s^2)\approx\frac{\nu_4-\nu_2^2}{N}-\frac{2(\nu_4-2\nu_2^2)}{N^2}+\frac{\nu_4-3\nu_2^2}{N^3}, \tag{20}$$

where the ν_q are the q sample moments from the mean,

$$\nu_q(t,x)=\frac{1}{N}\sum_r^N\left(\sum_i^{J'}\phi_i(x)\left(u_i(t,q_r)-\frac{1}{N}\sum_s u_i(t,q_s)\right)\right)^q. \tag{21}$$

4.5. Sample size. Accuracy of the statistical hypothesis

Sample size affects the determination of the accuracy of the mean and standard deviation. The deceiving dependence on $N^{1/2}$ and $N^{1/4}$ of Monte Carlo method in Eqs. (18) and (19) is an example of this. Also – more significant for this section –, it affects how good the assumption on the sample distribution is fulfilled. Note that if our own precondition is not fulfilled, in our case the $N_{tr}(\mu,\sigma,a,b)$ sample distribution, no effective conclusions can be obtained.

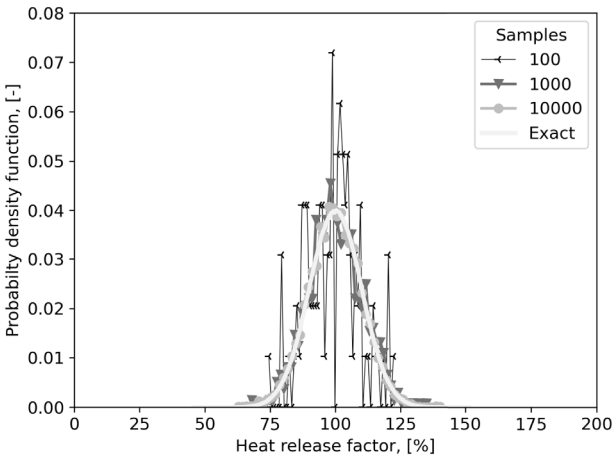

(a) $\sigma=0.1$.

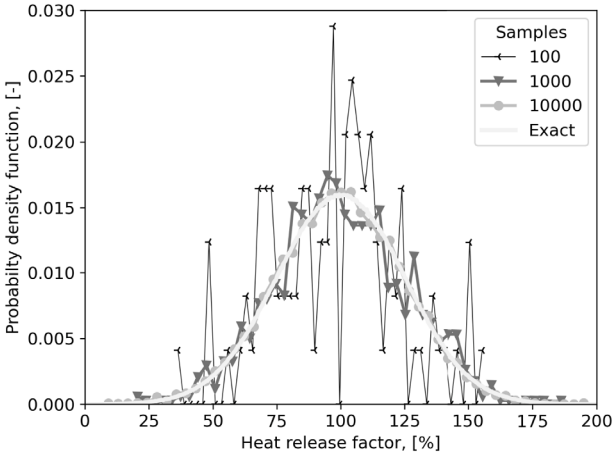

(b) $\sigma=0.25$.

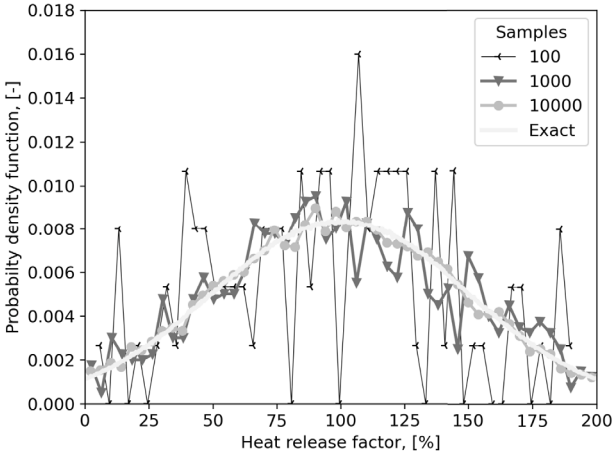

(c) $\sigma=0.5$.

Fig. 6. Measured probability density function.

Therefore, the effect of sample size on the adjustment to the intended distribution premise has been shown in Fig. 6.

In this diagram we compare the histograms constructed for three samples of size 100, 1000 and 10 000 with the theoretical results that

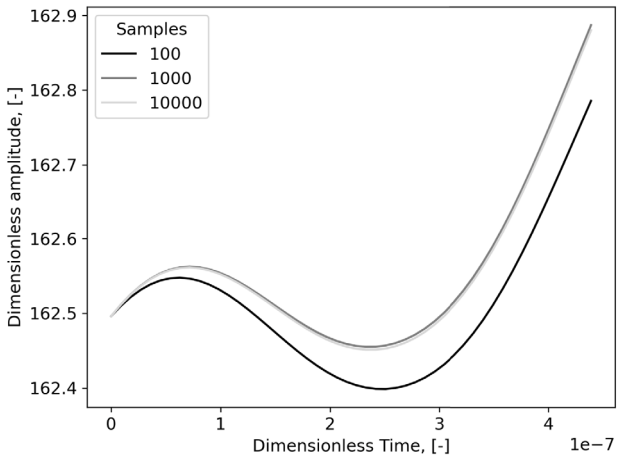

(a) First mode.

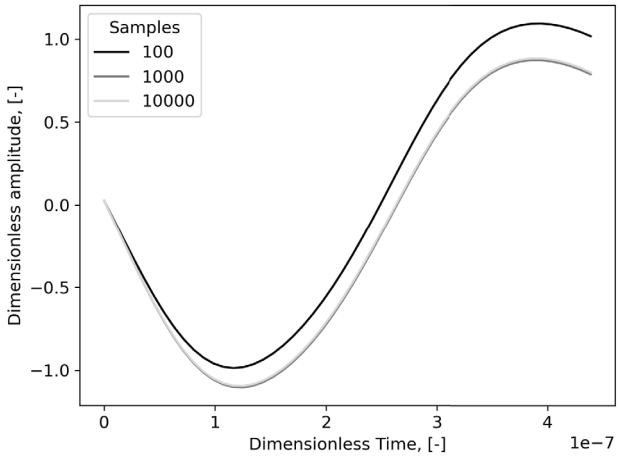

(b) Third mode.

Fig. 7. Amplitudes of the first and third ROM mode of temperature for $\sigma = 0.5$ and different samples.

should be obtained for $N_{tr}(\mu, \sigma, -1/\sigma, 1/\sigma)$ for values of sigma 0.1, 0.25 and 0.5.

Note the quite regular approximation that is achieved with the sample of the lowest size. The adjustment is even bad for the lowest of the standard deviations. In spite of it, with the lowest of the sigma values a reduced sample may produce meaningful results. The moments from the mean, namely 100%, grow with the value of sigma. The error induced in the histogram for the highest sigma is large in therms of the moments (integral areas).

The approximation achieved with samples with 10 000 points is very good, virtually indistinguishable form the exact value, for $\sigma = 0.1$ and $\sigma = 0.25$. For $\sigma = 0.5$ it is possible to distinguish the two curves. Still, its divergences are minimal.

The intermediate sample, with 1000 specimens, represent a compromise between the exactness of the large example –and its numerical overhead– and the roughness of the small –with its reduced accuracy–. It shows significant deviations from the exact values. On the other side, the deviations constitute an oscillation among the correct values, which global result should be acceptable.

We may see this concretely considering the average amplitudes of the modes of the ROM, term between brackets in Eq. (14). This magnitude has been represented in Fig. 7 for temperature.

Note that to the deviations represented in Fig. 6, the average amplitudes of Fig. 7 do not converge for the smaller sample. This happens both for the first mode 7(a) as well as for the third 7(b). Observe also that at the same time, the results obtained for the medium and the large examples are completely superimposed. That is, the medium size sample manages to produce a result that converges.

4.6. Main results

Utilization of the formula (14) for the results obtained with 10 000 samples with $\sigma = 0.5$ produces the mean fields shown in Fig. 8. In these figure, we see the evolution of the transient temperature, in the whole interval of 50 s, among the initial 150 s to the final 200 s.

Usage of the equivalent equation for the variance (15) produces also a field. Here, we have chosen to show the square root of the variance, the standard deviation, for its simpler interpretation, which has been represented in Fig. 9, for the temperature at different times for $\sigma = 0.5$ and 10 000 calculations.

For each figure, two presentations are included. On the right side, two cuts of the field are portrayed. On the left side, ten iso-surfaces are depicted. Note the complex pattern and local variation of this magnitude and therefore the uneven distribution of the error.

Take notice of the evolution of the relative distribution of the standard deviation and of its magnitude. Initially, the pattern is quite widespread, while it apparently concentrates with the increase of time. Note that the magnitude of the variable very significantly increases with time. This evolution is completely natural considering the conditions of the experiment. In our considerations, we accept the initial conditions are exactly know, but regard as uncertain the heat release of the sources. That is, the evolution is regarded as undetermined.

The evolution of the maximum of the standard deviation and thus of the scales of the patterns of Fig. 9 can be seen in Fig. 10. Note the significant increment of the times in the values reached for this magnitude. Also the fact that the values obtained for the three samples are nearly coincident in spite of the disparities of the sample's size.

Recall that the uncertainty of the mean – in its probabilistic assessment –, and thus the incertitude of the average, Fig. 7, is represented by the fields of Fig. 9, re-scaled by the factor $3/\sqrt{N}$, see Eq. (18).

Finally, we represent the evolution of the accuracy of the standard deviation of the temperature field, obtained for $\sigma = 0.5$ and 10 000 samples. By this accuracy is understood as the maximum probability bound of Eq. (19), $\sqrt{3}\sqrt[4]{Var_{sample}(s^2)/N}$, that was depicted in Fig. 11.

Note the unequal distribution of the bound as well as the increasing magnitude of the accuracy with the growth of time. The evolution of the scale of the magnitude with time can be better observed studying Fig. 12. We see there, how importantly the size of the sample affect the verisimilitude of the standard deviation.

4.7. Performance

4.7.1. Taxonomy of computational cost

In previous section the accuracy of the results obtained with different amount of samples was compared. Certainly, the experiments carried out with an enhanced amount of instances are superior in accuracy to the ones with a more modest amount of tests. Clearly, this accuracy comes in parallel with an enhanced amount of numerical burden.

Let us have a look on the computational cost of the methodology. In terms of machine power, the ROM procedure can be initially divided into two parts. The first, the *offline* phase mainly consists on the creation of the ROM. It has been described in detail (Yanez and Class, 2022) and is of no concern for this document. The second, the *online* stage regards the calculations, that is the utilization of the ROM for statistical purposes.

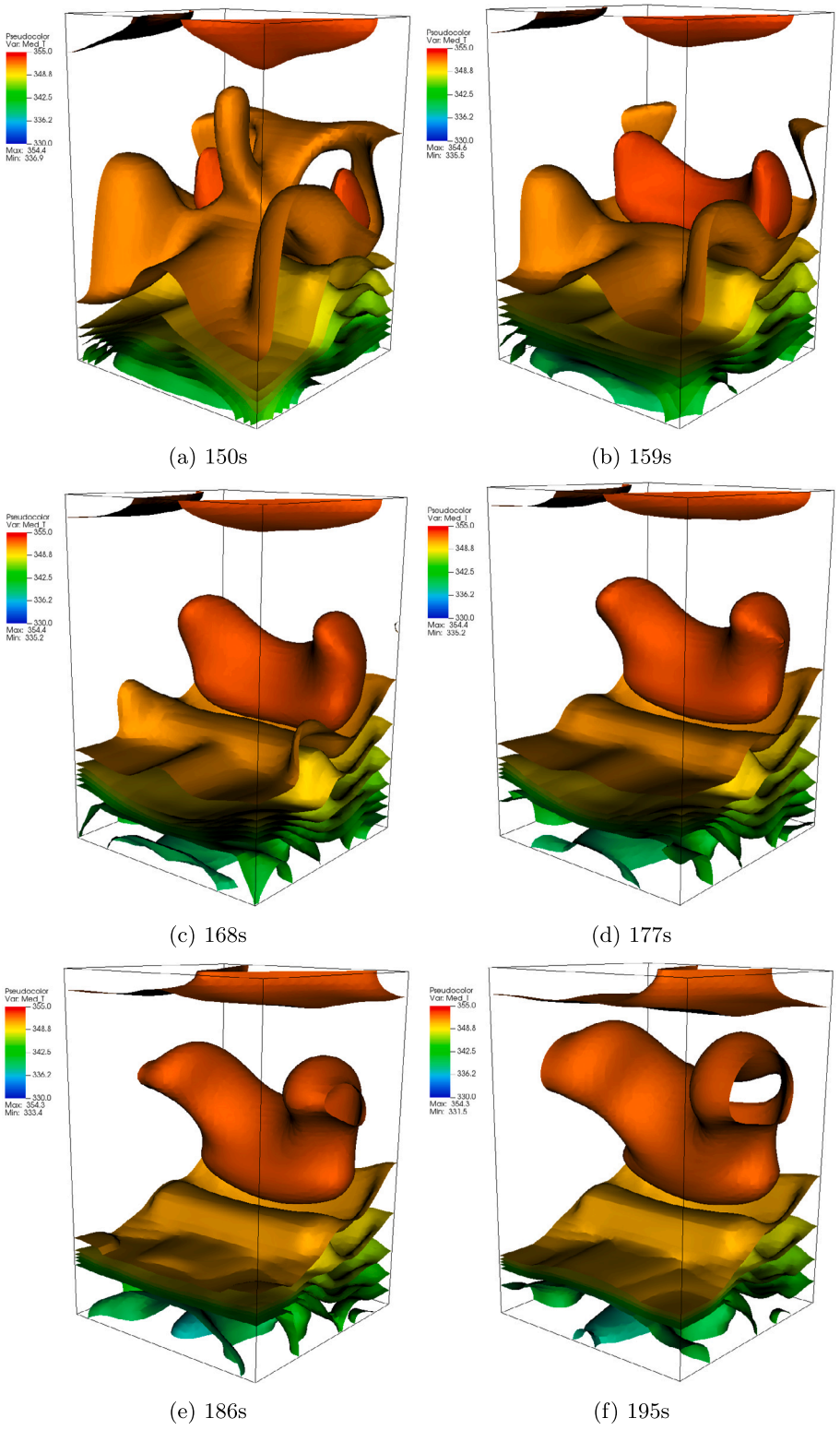

Fig. 8. Average results of temperature, $\sigma = 0.5$, 10 000 calculations.

The latter can, in turn, be divided into two parts: (I) Phase I: It concerns the performance of the calculations themselves, obtaining the amplitudes of the modes of the reduced basis by integration of the ROM, Eq. (9), in the conditions pertinent for the particular task in hand. (b) Phase II: It pertains the post-processing of the results for the derivation of the relevant statistical magnitudes – that may differ for each particular problem –, such as the ones described by Eqs. (14)–(15) and (18)–(21).

4.7.2. *Numerical performance of the statistical experiment*

The performance of our model and its implementation for the *online* stage can be seen in Table 1 for the cases that have been the object of the discussion of the paragraphs above.

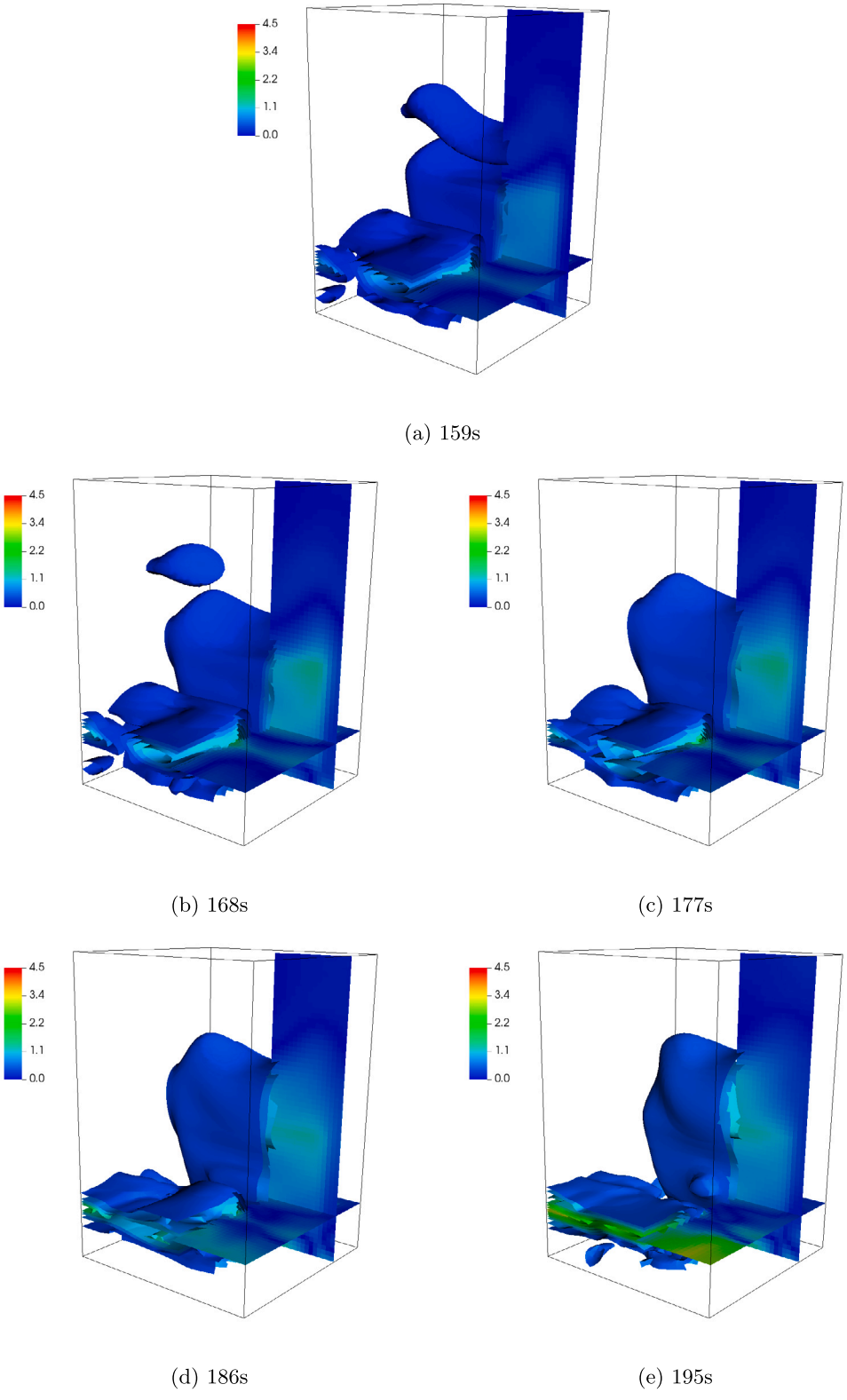

(a) 159s

(b) 168s

(c) 177s

(d) 186s

(e) 195s

Fig. 9. Standard deviation of temperature, $\sigma = 0.5$, 10 000 calculations.

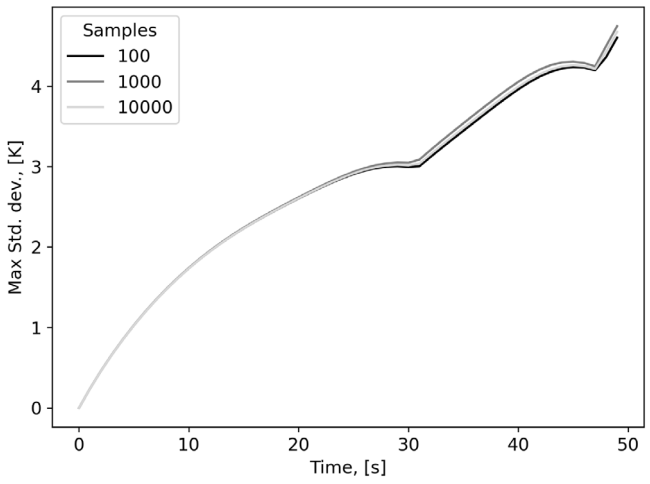

Fig. 10. Evolution of the maximum of the standard deviations for several samples, obtained for the temperature for the case $\sigma = 0.5$.

4.7.2.1. Numerical cost of Phase I. The results obtained for this stage the online phase corresponds to the second and third column of Table 1 and coincide with the time spend in integration of the ROM.

The computation overhead accounts for the solution of the system (9) and the computation of its matrices components $\mathbb{D}$, $\mathbb{E}$, $\mathbb{G}$. Note that these should be, at least partially, recalculated each time step, see Yanez and Class (2022). This recalculation is based – at least in part – on pre-computed blocks and can be done efficiently. In spite of the effective implementation, this constitutes a bothersome specificity. Nevertheless, it is intrinsically due to the non-linearity of the original equation system, see Yanez and Class (2022) for further details.

The individual ROM runs are, from the point of view of usage of memory, relatively small. The matrices of Eq. (9) are finally only 94×94. Therefore, independent runs are better carried out separately in a single processor. Parallelism can be more efficiently and simply achieved, launching several runs at same time, which number depends on the characteristics of the computer utilized, in our case, a machine with 8 Intel Core i7-3770, 3.40 GHz processors. In the table, for the purposes of comparison, the time shown is *serialized*, that is, expressed as if only a single processor was involved in all computations. Note that in the actual implementation the consumed time per run is of the order of 2.5 s. Such performance has been reached after a significant code profiling for efficiency.

4.7.2.2. Numerical cost of Phase II. The figures portraying the time required to post process the results and derive the pertinent statistical information is shown in last column of the Table 1.

The outcome of the post-processing include the mean, standard deviation and the corresponding accuracy of these variables, Eqs. (14)–(15) and (18)–(21). This has been carried out for the same numbers of times at which the snapshots where collected, namely 50.

The time expend in the post-processing stage is comparable to the ROM running time. This may appear as surprising, considering the simplicity of the statistical procedure, compared with the complexity of the ROM. To understand this fact one need to regard the nature of Eqs. (14) and e.g. (21). One can see that in the former, complexity is $N \cdot J' \cdot n$ and in the latter $N \cdot J' \cdot n \cdot log(q)$. That is Eqs. (14)–(15) and (18)–(21) have a dependence on n, and thus a significant larger complexity than the dimensions of the ROM.

4.7.3. Supplementary numerical experiment

We propose now a secondary exercise to study the performance of the ROM related to the results shown previously.

We reduce the domain of interest of power release from 0%–200% to 0%–100%. We consider *half* Gaussian distribution of heat release factor, that is $N_{tr}(0, \sigma, -1/\sigma, 0)$, that is, centered on 100% but having only the negative tail. We apply to this experiment our ROM model, constructed based on snapshots covering the range 0%–200% of heat release. We also build a second ROM model, this time constructed utilizing the same database, but based only the snapshots corresponding to 0%–100%. This second model is build with the same procedure as the first one and thus we do not repeat any details here. We do the same for the interval 100%–200%.

Because fewer snapshots are involved in the narrower intervals the new ROMs reduced basis contain fewer vectors. This has been illustrated in Table 2. Note that the construct intended for 0%–100% has 35% fewer modes than the full model whilst the one for 100%–200% just 32%.

The matrices of ROM systems, like the one of Eq. (9), are dense and has the dimensions of the reduced order system $J' \times J'$. Note that in contrast high accuracy solvers do mostly have sparse matrices but of dimensions n. Because of this squared dependence, a relatively small reduction in J' represents a very significant relief, see last column in Table 2. This amounts for a 55% and 58% increase of performance.

We may try to see the previous influence in terms of the implemented models, that also include additional overhead necessary to perform the calculations. The comparison of the calculation times of the full ROM and the restricted ROMs are included in Tables 3 and 4. Note that the time necessary for the completion of a single run is reduced by a 65% due to the selection of the restricted model, what is completely coherent with the previous statements. The computation time (also that of statistic derivation), are obtained considering *serial* computation, that is disregarding parallelization.

Note also that probably due to the load of the system, the time required to post process the solutions and obtain the statistics is slightly larger than the computation time.

Parallelization of the statistics extraction, that regards a single time for all the computations, is very effective, and is actually mostly limited by the usage of memory that the accumulation of solutions may require. RAM limitations were severe for the post-processing of the numerical experiment containing 10 000 samples, see Table 1. Therefore, an alternative more advanced post-processing routine was created to reduce memory consumption based on *Cython* (Behnel et al., 2011).

Table 1
Performance of the numerical experiments.

σ	Calcs.	Time, [s]	Time/Calc., [s]	Statistics time, [s]
0.1	100	246	2.4	66
0.25	100	254	2.5	52
0.5	100	240	2.4	52
0.5	1000	2458	2.4	2596
0.5	10 000	23 744	2.3	7474

Table 2
Amount of reduced basis vectors per variable.

Model	V	T	k	ϵ	Total	Squared
0%–200%	24	16	26	28	96	9216
0%–100%	16	11	17	18	62	3844
100%–200%	16	10	18	21	65	4225

Table 3
Performance of the numerical experiments, 0%–100% branch.

σ	Calcs.	Time, [s]	Time/Calc., [s]	Statistics time, [s]
Full model				
0.1	1000	2719	2.7	3719
0.25	1000	2664	2.6	3638
0.5	1000	2629	2.6	3632
Reduced model				
0.1	1000	1092	1.0	2326
0.25	1000	903	0.9	2176
0.5	1000	899	0.8	2301

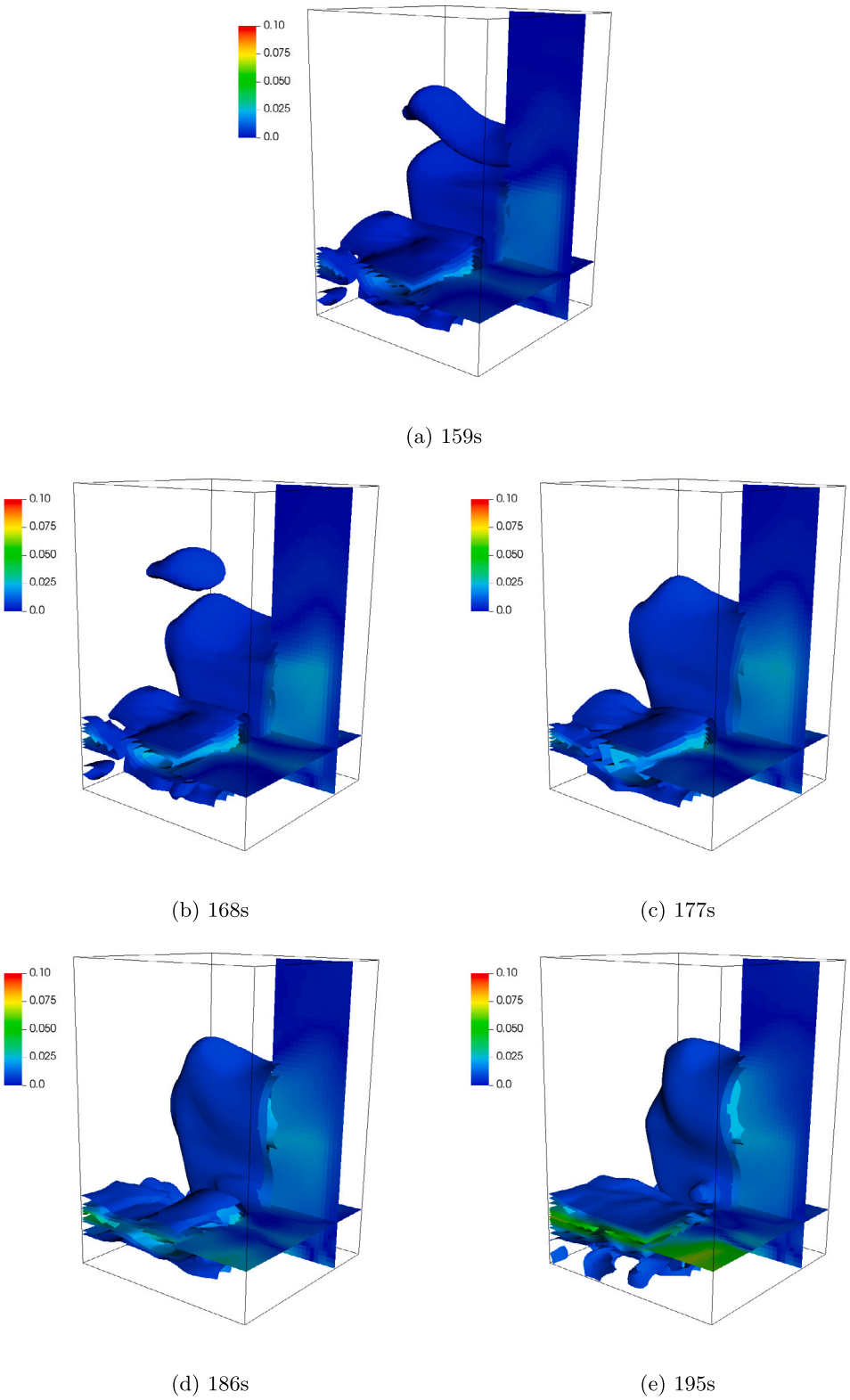

(a) 159s

(b) 168s

(c) 177s

(d) 186s

(e) 195s

Fig. 11. Accuracy of the standard deviation of temperature, $\sigma = 0.5$, 10 000 calculations.

5. Summary and conclusions

This article describes a statistical exercise utilizing our ROM of the standard $k - \epsilon$ turbulence model, for the analysis of the effect of a random variable in the result of a natural convention calculation. Thus, it constitutes an analogue to the papers (Yanez and Class, 2021b,a) with turbulence modeling included.

In this case, we conventionally regard the heat released by spent fuel elements as random and study the effect of this on the mean, standard deviation, and accuracy of the standard deviation. The model has been

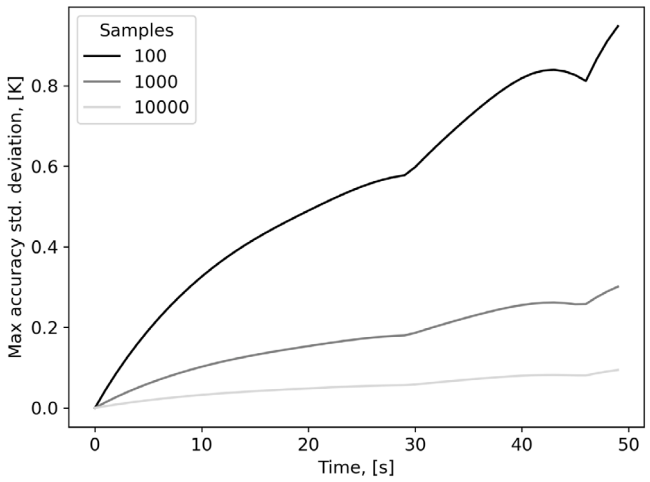

Fig. 12. Maximum interval of accuracy of the standard deviation for T, for $\sigma = 0.5$ and different samples.

Table 4
Performance of the numerical experiments, 100%–200% branch.

σ	Calcs.	Time, [s]	Time/ Calc., [s]	Statistics time, [s]
Full model				
0.1	1000	2964	2.9	3175
0.25	1000	3022	3.0	3188
0.5	1000	2935	2.9	2597
Reduced model				
0.1	1000	977	0.9	2337
0.25	1000	1084	1.0	2172
0.5	1000	1141	1.1	2104

created in a conventional manner, utilizing the known techniques of Proper Orthogonal Decomposition and Galerkin projection, following our previous developments in Yanez and Class (2022).

The application presented here concerns spent fuel refrigeration pools. But this is just a demonstration problem. The procedure followed here is suitable – defining the particular statistical hypothesis for the case of interest – to treat other cases. Particularly, we regard it as effective tool to assess the uncertainty quantification of fast reactors utilizing incompressible refrigerants. Specifically, those where the Boussinesq approximation is reasonable, namely the Lead-Cooled Fast Reactor, the Molten Salt Reactor and the Sodium-Cooled Fast Reactor.

We have also studied the performance of the method, demonstrating the possibility of performing ten thousand calculations inside the working time of a day with a common desktop computer. This means, that from the point of computational power, the methodology is usable for practitioners. Besides, we have shown the important additional performance increase that one may obtain by usage of a focused statistical case, strictly bounding the experiment defining a restrictive statistical hypothesis.

In terms of sample size, it was confirmed that one should very carefully balance performance with accuracy. The adequacy of small samples to obtain significant statistical magnitudes, and fulfill the statistical hypothesis imposed, without unacceptable deviations is limited. Strict bounds that warranty the accuracy of the results are only achievable through the usage of the large samples. These bounds are nevertheless problem dependent regarding the accuracy necessary for a particular task.

Trial-error procedure quickly provided a fair assessment of the sizes of the necessary samples to verify the statistical hypothesis and achieve the accuracy requirements. Therefore, a practical way of assessing sample size is to carry out tentative calculations firstly, to arrive to an adequate compromise. Finally, performance can by highly improved, if necessary, restricting the extension of the statistical experiment.

CRediT authorship contribution statement

Jorge Yanez: Conceptualization, Methodology, Software, Formal analysis, Writing – original draft, Writing – review & editing. **Andreas G. Class:** Conceptualization, Supervision, Project administration, Funding acquisition.

Declaration of competing interest

The authors declare that they have no known competing financial interests or personal relationships that could have appeared to influence the work reported in this paper.

Data availability

Data will be made available on request.

Acknowledgment

We kindly acknowledge the Framatome Professional School.

References

Abderrahim, H.A., Baeten, P., De Bruyn, D., Heyse, J., Schuurmans, P., Wagemans, J., 2010. MYRRHA, a multipurpose hybrid research reactor for high-end applications. Nucl. Phys. News 20 (1), 24–28.
Alemberti, A., et al., 2020. Lead cooled fast reactors. In: Reference Module in Earth Systems and Environmental Sciences. Elsevier, Amsterdam, the Netherlands.
Behnel, S., Bradshaw, R., Citro, C., Dalcin, L., Seljebotn, D.S., Smith, K., 2011. Cython: The best of both worlds. Comput. Sci. Eng. 13 (2), 31–39.
Benner, P., Grivet-Talocia, S., Quarteroni, A., 2021. Model Order Reduction: Volume 1. De Gruyter.
Benner, P., Schilders, W., Grivet-Talocia, S., Quarteroni, A., Rozza, G., Miguel Silveira, L., 2020a. Model Order Reduction: Volume 2: Snapshot-Based Methods and Algorithms. De Gruyter.
Benner, P., Schilders, W., Grivet-Talocia, S., Quarteroni, A., Rozza, G., Miguel Silveira, L., 2020b. Model Order Reduction: Volume 3: Applications. De Gruyter.
Berkooz, G., Holmes, P., Lumley, J.L., 1993. The proper orthogonal decomposition in the analysis of turbulent flows. Ann. Rev. FLuid Mech. 25 (1), 539–575.
Chaturantabut, S., Sorensen, D.C., 2010. Nonlinear model reduction via discrete empirical interpolation. SIAM J. Sci. Comput. 32 (5), 2737–2764.
Drazin, P.G., Drazin, P.D., 1992. Nonlinear Systems, Vol. 10. Cambridge University Press.
Escanciano, J.Y., Class, A.G., 2019. POD-Galerkin modeling of a heated pool. Prog. Nucl. Energy 113, 196–205.
Galik, G., Kutis, V., Jakubec, J., Paulech, J., Sedlar, T., 2016. Thermo-hydraulics of spent fuel storage pool of nuclear reactor VVER 440.
Grishchenko, D., Jeltsov, M., Kööp, K., Karbojian, A., Villanueva, W., Kudinov, P., 2015. The TALL-3D facility design and commissioning tests for validation of coupled STH and CFD codes. Nucl. Eng. Des. 290, 144–153.
Hesthaven, J.S., Rozza, G., Stamm, B., et al., 2016. Certified Reduced Basis Methods for Parametrized Partial Differential Equations, Vol. 590. Springer.
Hung, T.-C., Dhir, V.K., Pei, B.-S., Chen, Y.-S., Tsai, F.P., 2013. The development of a three-dimensional transient CFD model for predicting cooling ability of spent fuel pools. Appl. Therm. Eng. 50 (1), 496–504.
Iollo, A., Lanteri, S., Désidéri, J.-A., 2000. Stability properties of POD–Galerkin approximations for the compressible Navier–Stokes equations. Theor. Comput. Fluid Dyn. 13 (6), 377–396.
Jang, H., Jung, B., Hwang, J., 2006. Cooling analysis of spent fuel pool with a CFD method. Emergency 212, 239-240.
Kroese, D.P., Taimre, T., Botev, Z.I., 2013. Handbook of Monte Carlo Methods. John Wiley & Sons.
Launder, B.E., Spalding, D.B., 1983. The numerical computation of turbulent flows. In: Numerical Prediction of Flow, Heat Transfer, Turbulence and Combustion. Elsevier, pp. 96–116.
Menter, F.R., 1994. Two-equation eddy-viscosity turbulence models for engineering applications. AIAA J. 32 (8), 1598–1605.
Merle-Lucotte, E., Heuer, D., Allibert, M., Ghetta, V., Brun, C.L., 2008. Introduction to the physics of molten salt reactors. In: Materials Issues for Generation IV Systems. Springer, pp. 501–521.
Moisseytsev, A., Sienicki, J., 2012. Dynamic simulation and control of the S-CO_2 cycle: From full power to decay heat removal. Adv. Therm. Hydraul. 52–60.
Quarteroni, A., Manzoni, A., Negri, F., 2015. Reduced Basis Methods for Partial Differential Equations: An Introduction, Vol. 92. Springer.

Quarteroni, A., Rozza, G., et al., 2014. Reduced Order Methods for Modeling and Computational Reduction, Vol. 9. Springer.
Sheu, T.W.-H., Lin, R.-K., 2011. Three-dimensional bifurcations in a cubic cavity due to buoyancy-driven natural convection. Int. J. Heat Mass Transfer 54 (1–3), 447–467.
Siemens, P., 2018. STAR-CCM+ user's manual.
Sobol, I., 1974. The Monte Carlo Method. Popular Lectures in Mathematics. ERIC.
Sobol, I.M., 2018. A Primer for the Monte Carlo Method. CRC Press.
Star, S.K., Spina, G., Belloni, F., Degroote, J., 2021a. Development of a coupling between a system thermal–hydraulic code and a reduced order CFD model. Ann. Nucl. Energy 153, 108056.
Star, S., Stabile, G., Rozza, G., Degroote, J., 2021b. A POD-Galerkin reduced order model of a turbulent convective buoyant flow of sodium over a backward-facing step. Appl. Math. Model. 89, 486–503.
Tennekes, H., Lumley, J., 1992. A first course in turbulence.
Vergari, L., Cammi, A., Lorenzi, S., 2020. Reduced order modeling approach for parametrized thermal-hydraulics problems: inclusion of the energy equation in the POD-FV-ROM method. Prog. Nucl. Energy 118, 103071.
Wang, J.R., Lin, H.T., Tseng, Y.S., Shih, C.K., 2012. Application of TRACE and CFD in the spent fuel pool of chinshan nuclear power plant. In: Applied Mechanics and Materials, Vol. 145. Trans Tech Publ, pp. 78–82.
Weller, H.G., Tabor, G., Jasak, H., Fureby, C., 1998. A tensorial approach to computational continuum mechanics using object-oriented techniques. Comput. Phys. 12 (6), 620–631.
Wilcox, D.C., 1988. Reassessment of the scale-determining equation for advanced turbulence models. AIAA J. 26 (11), 1299–1310.
Yakhot, V., Orszag, S., Thangam, S., Gatski, T., Speziale, C., 1992. Development of turbulence models for shear flows by a double expansion technique. Phys. Fluids A 4 (7), 1510–1520.
Yanez, J., Class, A.G., 2021a. Analysis of the accuracy of residual heat removal and natural convection transients in reactor pools. Nucl. Eng. Des. 378, 111151.
Yanez, J., Class, A.G., 2021b. Analysis of the accuracy of residual heat removal in Gen-IV reactors. Nucl. Eng. Des. 376, 111102.
Yanez, J., Class, A.G., 2022. Reduced order model of standard k-ϵ turbulence model. Comput. & Fluids 245, 105608.